

A comparison of functional summary statistics to detect anisotropy of three-dimensional point patterns

Farzaneh Safavimanesh^{*1} and Claudia Redenbach^{†2}

¹Department of Mathematical Sciences, Institute for Cognitive and Brain Sciences, Shahid Beheshti University, Iran

²Department of Mathematics, Technical University of Kaiserslautern, Germany

Abstract

The growing availability of three-dimensional point process data asks for a development of suitable analysis techniques. In this paper, we focus on two recently developed summary statistics, the conical and the cylindrical K -function, which may be used to detect anisotropies in 3D point patterns. We give some recommendations on choosing their arguments and investigate their ability to detect two special types of anisotropy. Finally, both functions are compared on some real data sets from neuroscience and glaciology.

Key words: conical K -function, cylindrical K -function, Poisson line cluster point processes, Matérn hard core point processes, random ball packing, polar ice, minicolumn hypothesis

1 Introduction

In some situations, the spatial correlation between the points in a point pattern is not only a function of the distances between the points, but also of the direction of the vector connecting them. Classical functional summary statistics such as Ripley's K -function or the nearest neighbor distance distribution function fail to detect such anisotropies. Hence, there is some interest in developing methods which allow for a detection and characterization of the degree of anisotropy in a spatial point pattern.

In the literature, the case of two-dimensional point patterns has been at the focus of interest up to now. Various approaches for anisotropy analysis have been introduced, including spectral methods (Bartlett, 1964; Mugglestone and Renshaw, 1996; Renshaw, 2002), wavelet transformations (D'Ercole and Mateu, 2013a,b, 2014), and an anisotropy test based on the asymptotic joint normality of the sample second-order intensity function (Guan *et al.*, 2006). In addition, directional versions of functional summary statistics have been introduced in Ohser and Stoyan (1981), Stoyan and Beneš (1991), Stoyan (1991), and Stoyan and Stoyan (1995). Moreover, Møller and Toftaker (2014) introduced geometric anisotropic pair correlation functions.

At least some of these methods may be transferred to the three-dimensional case in theory. In practice, however, their application might be hampered, e.g. by problems in finding a suitable partition of the unit sphere. Furthermore, the visualization and verification of results is more

^{*}f_safavimanesh@sbu.ac.ir

[†]redenbach@mathematik.uni-kl.de

challenging. Recently, two directional counterparts of Ripley's K -function for the analysis of three-dimensional point patterns were introduced. The common idea of both approaches is to replace the ball used in the definition of the K -function by a structuring element which is sensitive to direction. The motivation of the work in Redenbach *et al.* (2009) was to detect anisotropy introduced by the compression of a regular point pattern. For this purpose, the mean numbers of points contained in cones centered in the typical point and pointing to different directions were investigated. The motivating data sets were point patterns of bubble centers extracted from tomographic images of polar ice cores. In contrast, Møller *et al.* (2015) studied some data from neuroscience where the points are believed to be organized in linear columns. Hence, they decided to use a cylinder instead of a cone.

These examples illustrate how the development of methods may be triggered by the particular shape of anisotropy that should be detected. In the current paper, we want to investigate the generality of the two directional versions of the K -function. For this purpose, we will apply them to both real and simulated point patterns with different sources and various degrees of anisotropy.

In Section 2 we introduce the data sets used throughout the paper. Section 3 defines the conical and cylindrical K -functions. Based on a non-parametric isotropy test, some simulation-based recommendations on the parametrization of these summary statistics are given in Section 4. Finally, in Section 5, we apply these recommendations when comparing the functions in detecting the anisotropy in real pyramidal cell and ice data sets as well as realizations of models mimicking the structure of these data.

2 Data sets

In this section, we introduce the data sets used for the subsequent analyses. We start with presenting the real data studied in Møller *et al.* (2015) and Redenbach *et al.* (2009) providing the motivation for the development of the two versions of the directional K -function. To allow for an investigation of the performance of the methods under varying degrees of anisotropy, our analysis is extended to simulated data sets. The models are chosen to reproduce the type of anisotropy present in the neuroscience data and the ice, respectively.

2.1 Real data sets

2.1.1 Pyramidal cell point patterns

The first set of data consists of four samples containing the locations of the pyramidal cells from the Brodmann area 4 of the gray matter of the human brain collected by the Center for Stochastic Geometry and Advanced Bioimaging, Denmark. According to the minicolumn hypothesis in neuroscience (see e.g. Mountcastle (1957) and Rafati *et al.* (2015)), the point patterns are expected to be anisotropic due to the linear arrangement of the cells in a direction perpendicular to the pial surface of the brain, i.e, the xy -plane here. For more details on these data sets, see Rafati *et al.* (2015). A visualization of one sample is shown in Figure 1.

2.1.2 Ice data

The second set of data consists of a subset of the samples investigated in Redenbach *et al.* (2009). The point patterns consist of the center locations of air bubbles extracted from

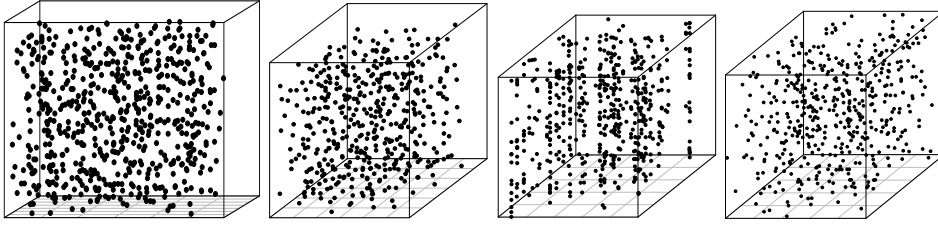


Figure 1: From left to right: a sample of the pyramidal data sets within an observation window of size $508 \times 140 \times 320 \mu\text{m}^3$, a sample of the ice data within an observation window of size $11.68 \times 11.92 \times 13.81 \text{ mm}^3$, a realization of the PLCPP model for $\rho = 500, \sigma = 0.001, \rho_L = 200, \alpha = 2.5$, and the compressed center locations of random ball packing for $\rho = 500, R = 0.05, c = 0.7$.

tomographic images of the Talos Dome ice core. The data were provided by the Alfred-Wegener-Institute for Polar and Marine Research, Bremerhaven, Germany. Details on the acquisition and the processing of the data can be found in Redenbach *et al.* (2009). Here, we consider 14 samples taken from a depth of 505 m where the anisotropy is most prominent. The point patterns can be interpreted as realizations of a regular point process. Anisotropy is introduced by a compression of the point pattern along the z -axis. Due to the location of the drilling site for this ice core, isotropy within the xy -plane can be assumed. A visualization of one sample is shown in Figure 1.

2.2 Simulated datasets

2.2.1 Poisson line cluster point processes

Motivated by the pyramidal cell data, a Cox process model called Poisson line cluster point process (PLCPP) for anisotropic spatial point processes was developed in Møller *et al.* (2015). The anisotropy of the realizations of this model is caused by linear arrangement of the points. For this purpose, we start with an anisotropic Poisson line process with intensity ρ_L and a given directional distribution of lines. On each line l_i contained in this process, a homogeneous Poisson process Y_i with intensity α is independently generated. Finally, the points of the Y_i are displaced in a plane orthogonal to l_i by e.g. a zero-mean normal distribution with the standard deviation σ yielding independent Poisson processes X_i whose superposition forms the PLCPP model X . The parameter σ controls the distances between the points and the lines. The intensity of X , i.e. the parameter ρ , is equal to the product of the intensity ρ_L of the Poisson line process and the intensity α of the Poisson processes Y_i on the lines.

Our investigations are based on PLCPP models with intensity $\rho = 500$, $\alpha = 2.5$, and $\rho_L = 200$, where the lines are parallel to the z -axis. We consider a high ($\sigma = 0.001$), medium ($\sigma = 0.01$), low ($\sigma = 0.02$), and very low ($\sigma = 0.04$) degree of linearity. Figure 1 shows a realization of a PLCPP model with a high degree of linearity. For the simulation study reported in the following, $m = 1000$ realizations were generated for each set of parameters.

2.2.2 Compressed regular point patterns

As discussed in Redenbach *et al.* (2009), the structure of the ice data can be modelled via compression of isotropic regular point processes. To represent different degrees of regularity, we consider both a Matérn hard-core process (low regularity, (Illian *et al.*, 2008, Section 6.5.2)) and the center locations of balls in a dense packing simulated using the force-biased

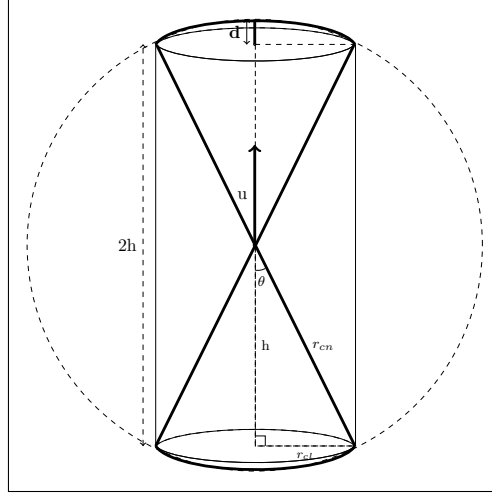


Figure 2: Structuring elements of the conical (the double cone) and the cylindrical (the cylinder) K -functions.

algorithm (high regularity, (Illian *et al.*, 2008, Section 6.5.5)). In both cases, the intensity was chosen as $\rho = 500$ and the hard core radius was $R = 0.05$. Anisotropy was then introduced by applying a volume-preserving linear transformation $T_c = \text{diag}(1/\sqrt{c}, 1/\sqrt{c}, c)$, $c \in [0, 1]$, to these isotropic regular point patterns. This implies that the data are compressed by a factor $0 < c < 1$ in z -direction while they are isotropically stretched by a factor $1/\sqrt{c}$ in the xy -plane.

As in the case of the PLCPP models, $m = 1000$ realizations for each model and each set of parameters were generated within the unit cube. Different degrees of compression were realized by choosing $c = 0.7, 0.8$, and 0.9 . Figure 1 shows a realization of a point pattern obtained from a ball packing compressed by a factor $c = 0.7$.

3 Conical and cylindrical K -functions

Ripley's K -function is a well-known summary statistic which is defined as the mean number of further points within a circle/sphere with radius r centered in a typical point of the point pattern divided by the intensity. Naturally, anisotropy cannot be detected using this function due to its symmetric structuring element. Redenbach *et al.* (2009) generalized the 2D directional K -function (see e.g. Stoyan and Stoyan (1995)) to the three-dimensional case by replacing the sector of a circle by a double cone. For a unit vector \mathbf{u} , the conical K -function is defined as

$$K_{\mathbf{u}, \text{cn}}(r_{\text{cn}}, \theta) = \frac{1}{\rho^2 |W|} \mathbb{E} \sum_{\mathbf{x}_1, \mathbf{x}_2 \in \mathbf{X}}^{\neq} \mathbf{1}[\mathbf{x}_1 \in W, \mathbf{x}_2 - \mathbf{x}_1 \in C_{\mathbf{u}}(r_{\text{cn}}, \theta)], \quad 0 < r_{\text{cn}}, 0 \leq \theta \leq \frac{\pi}{2}$$

where ρ is the intensity, and $C_{\mathbf{u}}(r_{\text{cn}}, \theta)$ denotes a double spherical cone in the direction \mathbf{u} with an slant height of length r_{cn} and an apex angle of size 2θ centered in 0 (see Figure 2). Briefly speaking, $\rho K_{\mathbf{u}, \text{cn}}(r_{\text{cn}}, \theta)$ is the mean number of further points within a cone $x_0 + C_{\mathbf{u}}(r_{\text{cn}}, \theta)$ centered in a typical point x_0 of the point pattern. In Redenbach *et al.* (2009) the function $K_{\mathbf{u}, \text{cn}}$ was called directional K -function. Here, we will call it conical K -function to distinguish it from the cylindrical K -function introduced below.

Møller *et al.* (2015) introduced a summary statistic, called the cylindrical K -function, to detect anisotropy of point patterns with columnar structure. It is a version of the space-time K -function (Diggle *et al.*, 1995) and is defined via

$$K_{\mathbf{u},\text{cl}}(r_{\text{cl}}, h) = \frac{1}{\rho^2 |W|} \mathbb{E} \sum_{\mathbf{x}_1, \mathbf{x}_2 \in \mathbf{X}}^{\neq} \mathbf{1}[\mathbf{x}_1 \in W, \mathbf{x}_2 - \mathbf{x}_1 \in Z_{\mathbf{u}}(r_{\text{cl}}, h)], \quad r_{\text{cl}}, h > 0,$$

where $Z_{\mathbf{u}}(r_{\text{cl}}, h)$ denotes a cylinder with center 0, base radius r_{cl} , and height $2h$ in the direction \mathbf{u} (see Figure 2). Briefly speaking, $\rho K_{\mathbf{u},\text{cl}}(r_{\text{cl}}, h)$ is the mean number of further points within a cylinder $x_0 + Z_{\mathbf{u}}(r_{\text{cl}}, h)$ centered in a typical point x_0 of the point pattern. For more details on the cylindrical K -function, see Møller *et al.* (2015).

Ratio-unbiased non-parametric estimates of the functions are, respectively, given by

$$\hat{K}_{\mathbf{u},\text{cn}}(r_{\text{cn}}, \theta) = \frac{1}{\hat{\rho}^2} \sum_{\mathbf{x}_1, \mathbf{x}_2 \in \mathbf{W}}^{\neq} w(\mathbf{x}_1, \mathbf{x}_2) \mathbf{1}[\mathbf{x}_2 - \mathbf{x}_1 \in C_{\mathbf{u}}(r_{\text{cn}}, \theta)]. \quad (1)$$

and

$$\hat{K}_{\mathbf{u},\text{cl}}(r_{\text{cl}}, h) = \frac{1}{\hat{\rho}^2} \sum_{\mathbf{x}_1, \mathbf{x}_2 \in \mathbf{W}}^{\neq} w(\mathbf{x}_1, \mathbf{x}_2) \mathbf{1}[\mathbf{x}_2 - \mathbf{x}_1 \in Z_{\mathbf{u}}(r_{\text{cl}}, h)]. \quad (2)$$

where n is the number of points in the point pattern, $\hat{\rho}^2 = n(n-1)/|W|^2$ is an unbiased estimate of ρ^2 (see e.g. Illian *et al.* (2008)), and w is the translation edge correction factor defined as

$$w(\mathbf{x}_1, \mathbf{x}_2) = 1/|W \cap W_{\mathbf{x}_2 - \mathbf{x}_1}|$$

in which $W_{\mathbf{x}}$ denotes the translation of the observation window W by the vector \mathbf{x} (see e.g. Stoyan and Stoyan (1995)).

Both estimators can easily be evaluated using a spherical or cylindrical coordinate system, respectively. However, unlike in the two-dimensional case, it is impossible to partition the unit sphere into equally sized cones or cylinders pointing to different directions. In practice, the directional K -functions can be evaluated for a set of directions evenly distributed on the unit sphere. Approaches for deriving such sets of directions are discussed in Altendorf (2011). If possible, the choice of the number of directions should be based on prior knowledge on the main directions of anisotropy.

While the classical summary statistics for point processes, e.g. Ripley's K -function, depend on one parameter, the summary statistics introduced above depend on two parameters which makes the investigations more challenging. For the cone, it seems natural to fix the parameter θ in advance such that the conical K -function only depends on the parameter r_{cn} . In practice, θ should be chosen depending on the number of directions to be investigated and the intensity of the point pattern. In Redenbach *et al.* (2009) an angle of $\theta = \frac{\pi}{4}$ was chosen when considering only coordinate directions. For larger sets of directions, θ should be reduced to avoid overlap of the cones for different directions. Additionally, the angle should be large enough to observe a reasonable number of points within the cones.

For the cylinder, the situation is more complicated as there are three ways to expand a cylinder (see Figure 3) depending on the two parameters r_{cl} and h . A priori, none of these methods seems more natural than the other. In Rafati *et al.* (2015), the height of the cylinder was fixed while expanding its radius. In the present study, we are interested in a comparison of the cylindrical and the conical K -function. Hence, the expansion scenario should be chosen such that both functions behave similarly in some sense. Two possible approaches are discussed in the following section.

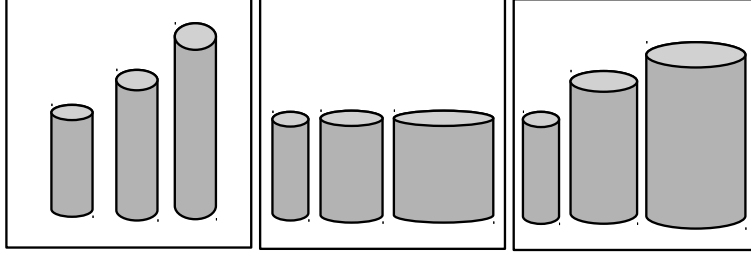


Figure 3: Three ways of expanding a cylinder when detecting the anisotropy in the point patterns: expanding h given a fixed r_{cl} (left panel), expanding r_{cl} given a fixed h (middle panel), or expanding both r_{cl} and h (right panel).

4 Choice of parametrization

4.1 Equal volume

The first parametrization is based on the fact that sets of equal volume will contain a similar number of points. Hence, we suggest to parametrize the functions such that the volumes of the cone and the cylinder are equal. The details are as follows.

Recall that r_{cn} and r_{cl} refer to the radius of the cone (or the radius of the circumscribed sphere), and the radius of the cylinder, respectively (see Figure 2). Knowing that the volume of a cylinder, a cone, and a spherical cap are, respectively, given by

$$V_{cl} = \pi r_{cl}^2 2h, V_{cone} = \frac{1}{3} \pi r_{cl}^2 h, V_{cap} = \frac{\pi d^2}{3} (3r_{cn} - d)$$

where $d = r_{cn} - h$ is the height of the cap, the volume of the double cone (used as the structuring element of the conical K -function) is given by

$$\begin{aligned} V_{cn} &= 2[V_{cone} + V_{cap}] \\ &= 2\left[\frac{1}{3} \pi r_{cl}^2 h + \frac{\pi}{3} (r_{cn} - h)^2 (3r_{cn} - (r_{cn} - h))\right] \\ &= \frac{1}{3} \pi r_{cl}^2 2h + \frac{2\pi}{3} (r_{cn} - h)^2 (2r_{cn} + h) \end{aligned}$$

Using the above formula, those values of r_{cn} , r_{cl} , and h satisfying

$$r_{cl}^2 2h = (r_{cn} - h)^2 (2r_{cn} + h). \quad (3)$$

lead us to the equation $V_{cn} = V_{cl}$, i.e., the equality of the volumes of the structuring elements of the two functions.

Equation (3) leaves two degrees of freedom. In practice, it can be accompanied by further constraints such as the choice of an aspect ratio for the cylinder (see below).

4.2 Equal shape

An alternative approach is to require that similar regions of the data are scanned in the sense that the shapes of the structuring elements are similar. This is achieved by placing the cone inside the cylinder as shown in Figure 2. In this case, the following equations hold:

$$\cot(\theta) = \frac{h}{r_{cl}} \quad (4)$$

and

$$r_{\text{cn}}^2 = h^2 + r_{\text{cl}}^2. \quad (5)$$

Following the recommendation given in Møller *et al.* (2015) on using an elongated cylinder, i.e. where $h > r_{\text{cl}}$, the right hand side of equation (4) can be considered as an aspect ratio. It is clear that when this ratio is equal to one, no anisotropy is expected to be detected by this function. Taking an aspect ratio $\cot(\theta) = a > 1$ and using equations (4) and (5) results in

$$h = ar_{\text{cl}} \quad (6)$$

and

$$r_{\text{cn}} = r_{\text{cl}}\sqrt{a^2 + 1} \quad (7)$$

which provides us with an alternative relationship between the three parameters r_{cn} , r_{cl} and h . In the following, we will use the parametrization based on equations (6) and (7).

4.3 Isotropy test

Redenbach *et al.* (2009) introduced a non-parametric method to detect anisotropies in the point patterns as follows. Assuming isotropy in the xy -plane and knowing that the anisotropy is directed along the z -axis, the isotropy test for m replicated point patterns is based on the statistics given by

$$T_{xy,i} = \int_{r_1}^{r_2} |\hat{S}_{x,i}(r) - \hat{S}_{y,i}(r)|dr$$

and

$$T_{z,i} = \min \left(\int_{r_1}^{r_2} |\hat{S}_{x,i}(r) - \hat{S}_{z,i}(r)|dr, \int_{r_1}^{r_2} |\hat{S}_{y,i}(r) - \hat{S}_{z,i}(r)|dr \right)$$

where $[r_1, r_2]$ is a given interval, and \hat{S}_x , \hat{S}_y , and \hat{S}_z are estimates of a summary statistic (here, either the conical or the cylindrical K -function) in the directions of the x -, y -, and z -axis, respectively. Here, r_{cl} or r_{cn} are chosen as the integration variable while the remaining parameters h and θ are chosen by any of the approaches discussed above.

In case of isotropy, these three estimates should behave similarly, while \hat{S}_z should be clearly different from \hat{S}_x and \hat{S}_y if the anisotropy is directed along the z -axis. Hence, the null hypothesis of isotropy will be rejected at significance level α if the value of $T_{z,i}$ corresponding to the i -th point pattern is larger than $100(1 - \alpha)\%$ of the estimated $T_{xy,i}$ values. The performance of the test is evaluated using its power, estimated by the average number of times the null hypothesis is rejected in 1000 repetitions of the test. Note that the values of r_1 and r_2 should be chosen depending on the type of anisotropy. We fix $r_1 = 0$ and will investigate the effect of different choices of r_2 on the power of the test (see also Redenbach *et al.* (2009)).

When using the equations obtained in the above sections, one should also decide on an appropriate aspect ratio a . Figure 4 shows plots of the power of the isotropy test at level 5% versus the parameter r_2 for the cylindrical K -function (and the corresponding r_2 for the conical K -function obtained using (7)) for the aspect ratios a from 1.5 to 3 with an increment of size 0.5, based on $m = 1000$ realizations under the PLCPP model introduced in Section 2.2.1.

The results indicate that the use of longer cylinders results in larger powers of the isotropy tests. This supports the recommendation given in Møller *et al.* (2015) on using an elongated cylinder. In each plot, the maximum is obtained for approximately the same r_2 value, no matter which h is chosen. For higher degrees of linearity, the power of the test is higher in general. Furthermore, it is less sensitive to the choice of r_2 .

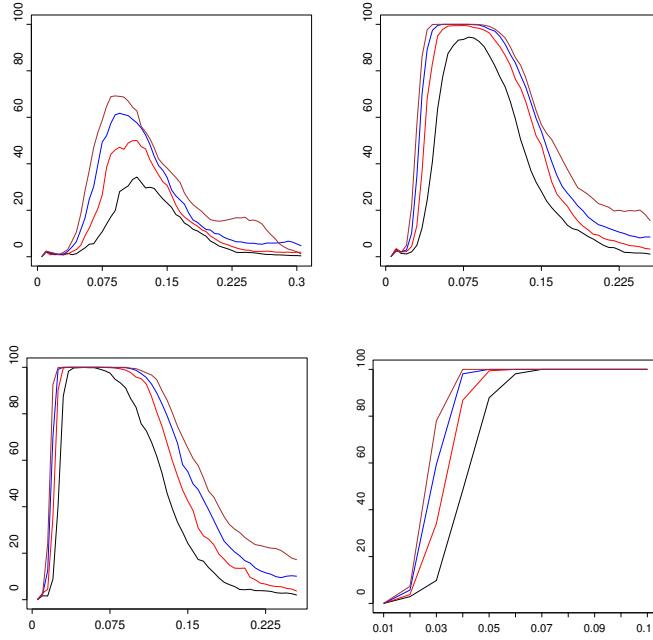


Figure 4: The power of the isotropy test at level 5% versus the parameter r_2 for the realizations of the PLCPP model with (from top left to bottom right) very low, low, medium, and high degree of linearity based on the cylindrical K -function. The curves from bottom (black) to top (brown) correspond to the aspect ratios from $a = 1.5$ to $a = 3$ with an increment of size 0.5.

5 Application

Even though the findings presented in the previous section suggest using a cylinder as long as possible, we have chosen an aspect ratio of $a = 2$ for the subsequent analyses. The reasons are as follows: When using a very long cylinder, serious edge effects may occur already for small values of r_{cl} resulting in poor estimates of the cylindrical K -function. In addition, increasing the length of the cylinder would mean to reduce the angle used for the cone. As we already mentioned, one should make sure that the cone is not too narrow as in this case it will only contain very few points.

Hence, in the applications, we chose $\theta = 0.4636476$ which is corresponding to $a = 2$, i.e. the case where the height of the cylinder is twice the diameter of its base. Figure 5 shows the means of the estimated values of conical and the cylindrical K -functions for 1000 realizations of the simulated data sets introduced in Sections 2.2.1 and 2.2.2. The mean values are obtained using the ratio estimation method described in Baddeley *et al.* (1993). The x -axis of the plot shows the values for r_{cl} (and the corresponding parameters r_{cn} and h are obtained from equations (6) and (7) to get comparable scales). With the exception of the Matérn case where the anisotropy is only weakly pronounced, both functions are able to detect the anisotropy. However, it is not easy to see which function is more sensitive to the structure of the anisotropy. Therefore, we made a comparison based on the power of the isotropy tests as follows.

The first four panels of Figure 6 show the plots of the powers of the isotropy test at a 5% significance level using $m = 1000$ simulations under the PLCPP models with four degrees of linearity as mentioned in Section 2.2.1. The plots indicate that the power of the anisotropy

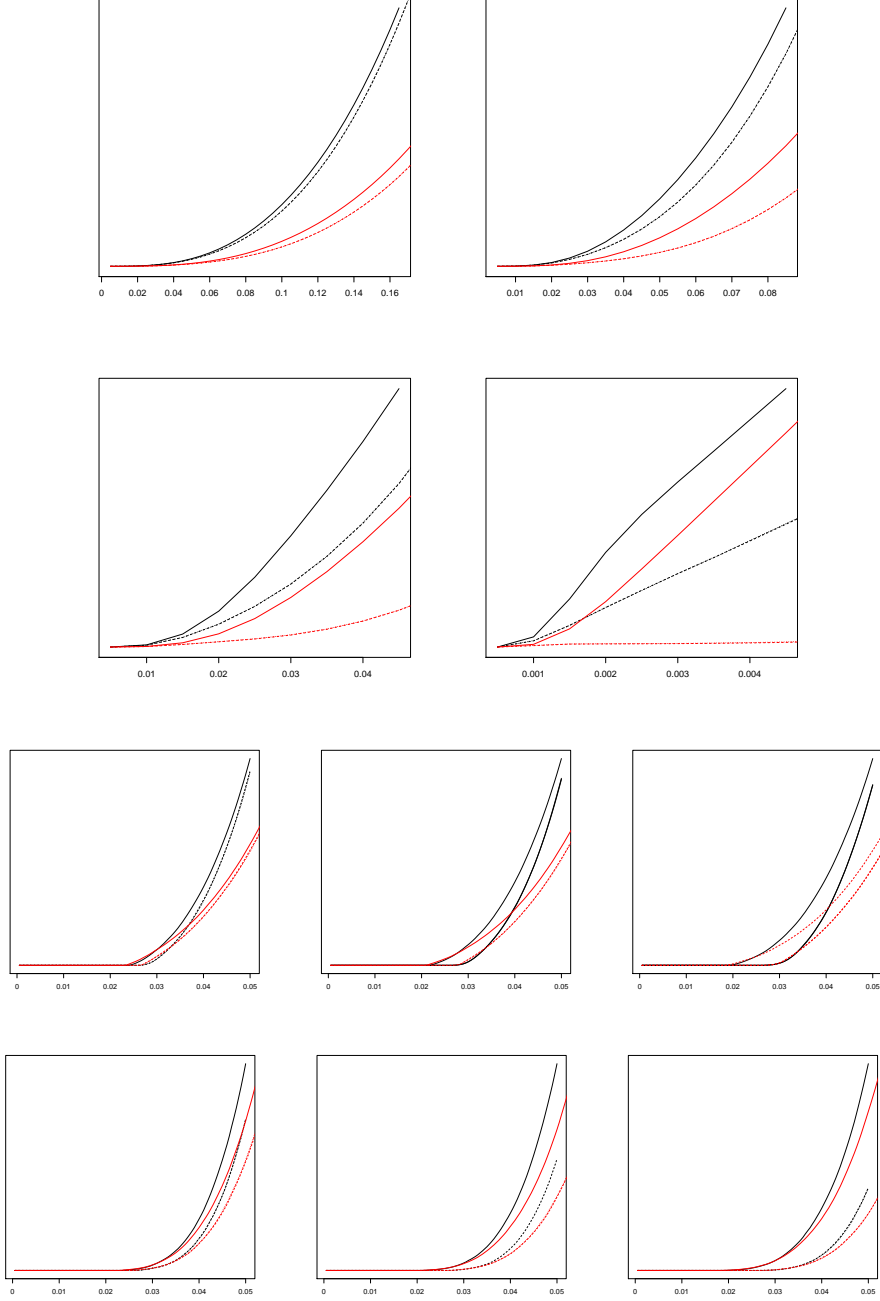


Figure 5: Means of the estimated values of the cylindrical (black) and conical (red) K -functions for the realizations of the PLCPP with $\sigma = 0.04, 0.02, 0.01, 0.001$ (first four panels from top left to bottom right), Matérn hard-core (third row), and random packing of balls (last row), in the direction of the z (solid), x (dotted), and y (dashed) axis. The order in the last two rows corresponds to the factors $c = 0.9, 0.8, 0.7$, from left to right, respectively.

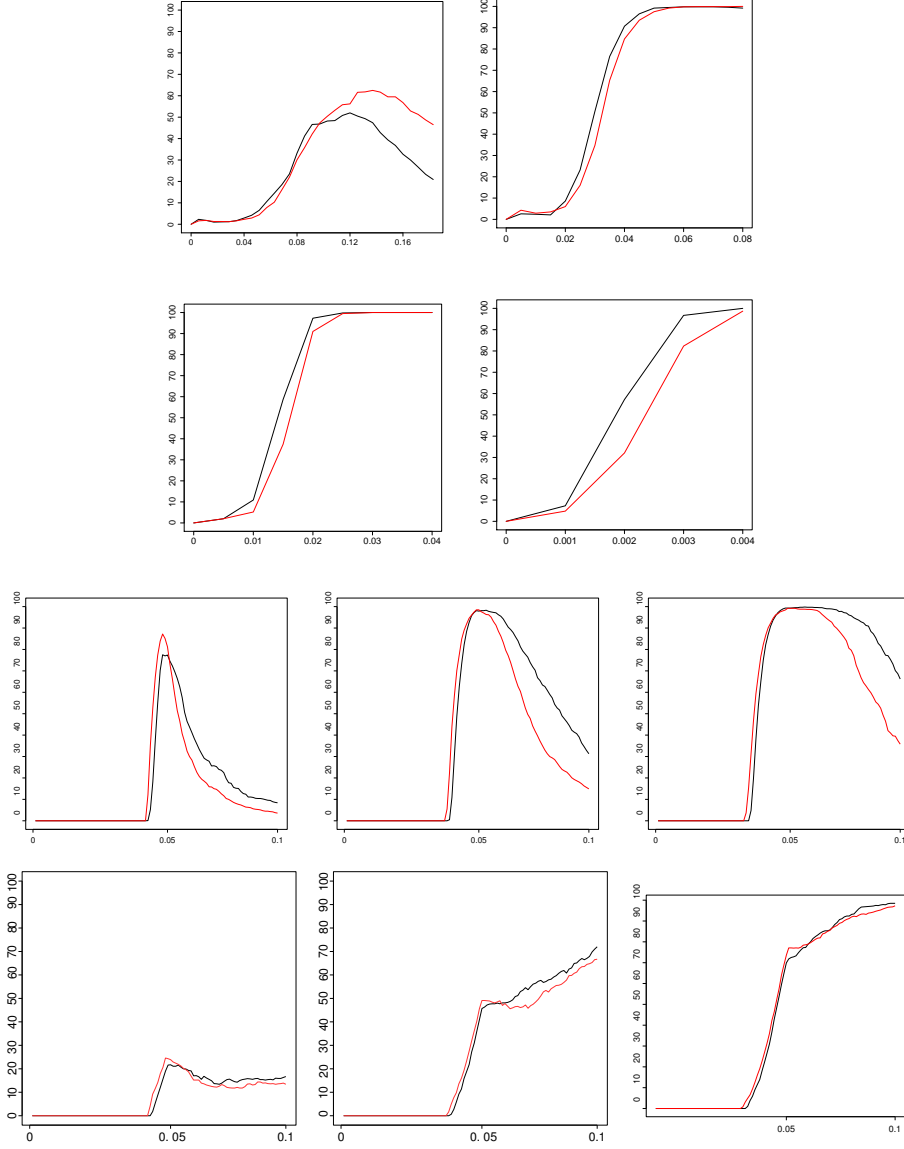


Figure 6: The powers of the isotropy test at level 5% as a function of r_2 with respect to r_{cl} when using the cylindrical (black) and conical (red) K -function, for the realizations of the PLCPP with $\sigma = 0.04, 0.02, 0.01, 0.001$ (first four panels from top left to bottom right), Matérn hard-core (third row), and random packing of balls (last row). The last two rows correspond to the factors $c = 0.9, 0.8, 0.7$, from left to right, respectively.

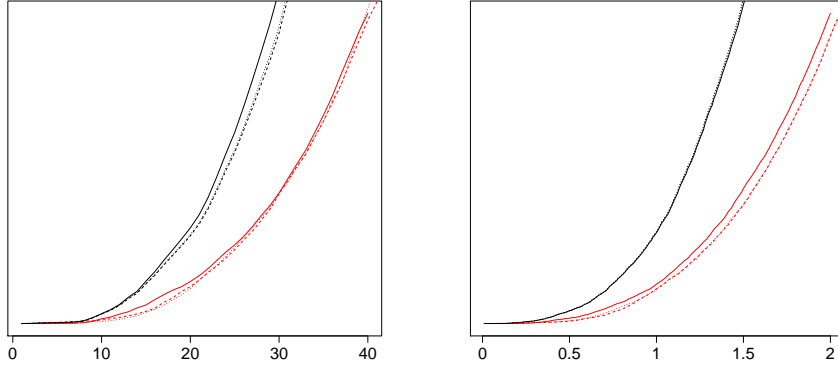


Figure 7: Estimates of the cylindrical (black) and the conical (red) K -function in the direction of the z (solid), x (dotted), and y (dashed) axis for a sample of the pyramidal cell data (left panel) and the ice data (right panel).

test is slightly higher when using the cylindrical K -function than when using the conical one. The shape of the two curves is similar in all plots. In contrast, the last two rows of this figure show that the conical K -function is more powerful than the cylindrical one in detecting the anisotropy caused by compression of the regular point patterns when choosing r_2 close to the hardcore radius while the cylindrical K -function is better for large r_2 .

Extra information provided by the plots is that the power of the test obtains its maximum where the whole column in the point patterns with columnar structure is captured. As an example to clarify this point, the fourth panel, which is corresponding to a realization of a PLCPP with $\sigma = 0.001$, satisfies our expectation of the diameter of a cylindrical cluster of points to be approximately $4\sigma = 0.004$ (by definition of the PLCPP models). This pattern is followed by the other three values of σ as well. In case of the regular point patterns, the maximum is obtained for r_2 close to the hardcore radius of $R = 0.05$ which corresponds to the findings in Redenbach *et al.* (2009).

Figure 7 shows the estimated K -functions for samples of the pyramidal cell and the ice data sets introduced in Sections 2.1.2 and 2.1.1 using the parametrization obtained in equations (6) and (7). As expected based on the power of the isotropy test, the conical K -function is more powerful than the cylindrical one in detecting the anisotropy in the ice data. On the other hand, the cylindrical K -function is stronger than the conical one in detecting the anisotropy caused by the linear arrangement of the pyramidal cells. Note that we obtained the same behavior when using the rest of samples.

6 Discussion

In this paper, we have presented a comparison of two directional versions of Ripley's K -function using a cone or a cylinder as structuring element. We derived a parametrization to make both functions comparable. Then, both functions were applied to data sets with different sources of anisotropy. The cylindrical K -function is generally more powerful than the conical one in case of columnar anisotropy and vice versa in case of compression. In situations where the anisotropy is clearly pronounced, although it can be detected by both functions, the cylindrical K -function is clearly more powerful than the conical K -function in detecting columnarity.

Our application examples show quite different model geometries: points clustered in linear patterns in the minicolumn data and compressed regular point patterns in the ice data. In order to get a comparable testing scenario, we decided to use the nonparametric setting suggested in Redenbach *et al.* (2009). While this approach is pretty general, it requires replicated data which are not always available in practice. Nevertheless, an investigation of plots of the directional K -functions for different directions may give an indication of existing anisotropies. In cases where a suitable model for the data is available, the test could be replaced by a model based Monte Carlo test.

The examples given in this paper emphasize the importance of an appropriate choice of the combination of the parameters (r_{cl}, h) and (r_{cn}, θ) as well as the integration interval in the test. An unfavorable choice may result in a poor performance of the functions in detecting the anisotropy of a point pattern. In practical situations, prior information on the construction of the anisotropy, e.g. the diameter of the clusters of points in case of the pyramidal cells or the hardcore radius in the regular data, can be used to determine interesting ranges of r values.

Throughout this paper, we assume that the main anisotropy directions are known and fixed. An approach for estimating the main directions in case of the cylindrical K -function was discussed in Møller *et al.* (2015). A similar investigation for the ice data has been done in Rajala *et al.* (2016).

Acknowledgments

This project was supported by the Danish Council for Independent Research | Natural Sciences, grant 12-124675, ‘Mathematical and Statistical Analysis of Spatial Data’, by the Centre for Stochastic Geometry and Advanced Bioimaging, funded by a grant from the Vilum Foundation, and by the Center for Mathematical and Computational Modelling (CM)² funded by the state of Rhineland-Palatinate, Germany.

We thank Jens Randel Nyengaard, Karl-Anton Dorph Petersen, and Ali H. Rafati at the Center for Stochastic Geometry and Bioimaging (CSGB), Denmark, for collecting the 3D pyramidal cell data, and Johannes Freitag, Alfred-Wegener Institute Bremerhaven, for providing the polar ice data.

References

- Altendorf, H. (2011). *3D Morphological Analysis and Stochastic Modeling of Random Fiber Networks - applied on Glass Fiber Reinforced Composites..* Ph.D. thesis, Mines ParisTech and TU Kaiserslautern.
- Baddeley, A. J., Howard, C. V. & Boyde, A. (1993). Analysis of a three-dimensional point pattern with replication. *Journal of Applied Statistics* **42**, 641–668.
- Bartlett, M. (1964). The spectral analysis of two-dimensional point processes. *Biometrika* **51**, 299–311.
- D’Ercole, R. & Mateu, J. (2013a). A continuous wavelet-based approach to detect anisotropic properties in spatial point processes. *International Journal of Wavelets, Multiresolution and Information Processing* **11**, 1350017–1350046.
- D’Ercole, R. & Mateu, J. (2013b). On wavelet-based energy densities for spatial point processes. *Stochastic Environmental Research and Risk Assessment* **27**, 1507–1523.

- D'Ercole, R. & Mateu, J. (2014). A wavelet-based approach to quantify the anisotropy degree of spatial random point configurations. *International Journal of Wavelets, Multiresolution and Information Processing* **12**, 1450037–1450059.
- Diggle, P., Chetwynd, A., Häggkvist, R. & Morris, S. (1995). Second order analysis of space-time clustering. *Statistical Methods in Medical Research* **4**, 124–136.
- Guan, Y., Sherman, M. & Calvin, J. (2006). Assessing isotropy for spatial point processes. *Biometrics* **62**, 119–125.
- Illian, J., Penttinen, A., Stoyan, H. & Stoyan, D. (2008). *Statistical Analysis and Modelling of Spatial Point Patterns*. John Wiley and Sons, New York.
- Møller, J. & Toftaker, H. (2014). Geometric anisotropic spatial point pattern analysis and Cox processes. *Scandinavian Journal of Statistics* **41**, 414–435.
- Møller, J., Safavimanesh, F. & Rasmussen, J. G. (2015). The cylindrical k -function and the poisson cluster line point processes. Submitted for publication, Available at arXiv:1503.07423.
- Mountcastle, V. B. (1957). Modality and topographic properties of single neurons of cat's somatic sensory cortex. *Journal of Neurophysiology* **20**, 408–434.
- Mugglestone, M. & Renshaw, E. (1996). A practical guide to the spectral analysis of spatial point processes. *Computational Statistics & Data Analysis* **21**, 43–65.
- Ohser, J. & Stoyan, D. (1981). On the second-order and orientation analysis of planar stationary point processes. *Biometrical Journal* **23**, 523–533.
- Rafati, A., Safavimanesh, F., Dorph-Petersen, K., Rasmussen, J. G., Møller, J. & Nyengaard, J. R. (2015). Detection and spatial characterization of minicolumnarity in the human cerebral cortex. *Journal of Microscopy* **261**, 115–126.
- Rajala, T. A., Särkkä, A., Redenbach, C. & Sormani, M. (2016). Estimating geometric anisotropy in spatial point patterns. *Spatial Statistics* **15**, 139–155.
- Redenbach, C., Särkkä, A., Freitag, J. & Schladitz, K. (2009). Anisotropy analysis of pressed point processes. *AStA Advances in Statistical Analysis* **93**, 237–261.
- Renshaw, E. (2002). Two-dimensional spectral analysis for marked point processes. *Biometrical Journal* **44**, 718–745.
- Stoyan, D. (1991). Describing the anisotropy of marked planar point process. *Statistics: A Journal of Theoretical and Applied Statistics* **22**, 449–462.
- Stoyan, D. & Beneš, V. (1991). Anisotropy analysis for particle systems. *Journal of Microscopy* **164**, 159–168.
- Stoyan, D. & Stoyan, H. (1995). *Fractals, Random Shapes and Point Fields*. John Wiley and Sons, Chichester.